Acta Cryst. (1999). B**55**, 273–284

Electron density distribution and Madelung potential in α-spodumene, $LiAl(SiO_3)_2$, from two-wavelength high-resolution X-ray diffraction data

Sandrine Kuntzinger and Nour Eddine Ghermani*

Laboratoire de Cristallographie et Modélisation des Matériaux Minéraux et Biologiques, LCM^{3}B, UPRES A CNRS 7036, Université Henri Poincaré, Nancy 1, Faculté des Sciences, Boulevard des Aiguillettes, BP 239, 54506 Vandoeuvre-lès-Nancy CEDEX, France. E-mail: ghermani@lcm3b.u-nancy.fr

(*Received 3 July 1998; accepted 15 October 1998*)

Abstract

The electron density distribution in α-spodumene, $LiAl(SiO_3)_2$, was derived from high-resolution X-ray diffraction experiments. The results obtained from both Mo $K\alpha$- and Ag $K\alpha$-wavelength data sets are reported. The features of the Si—O and Al—O bonds are related to the geometrical parameters of the Si—O—Al and Si—O—Si bridges on the one hand and to the O$\cdots$Li$^+$ interaction on the other. Kappa refinements against the two data sets yielded almost the same net charges for the Si (+1.8 e) and O (−1.0 e) atoms in spodumene. However, the Al net charge obtained from the Ag $K\alpha$ data (+1.9 e) is larger than the net charge derived from the Mo $K\alpha$ data (+1.5 e). This difference correlates with a more contracted Al valence shell revealed by the shorter X-ray wavelength (κ = 1.4 for the Ag $K\alpha$ data set). The derived net charges were used to calculate the Madelung potential at the spodumene atomic sites. The electrostatic energy for the chemical formula $LiAl(SiO_3)_2$ was -8.60 e^2 Å^{-1} (-123.84 eV) from the net charges derived from the Ag $K\alpha$ data and -6.97 e^2 Å^{-1} (-100.37 eV) from the net charges derived from the Mo $K\alpha$ data.

1. Introduction

In our investigation of the electrostatic properties of minerals, the pyroxene group offers the opportunity to study a structure with O-atom-corner-connected Si tetrahedra in infinite parallel chains. Only one of the three O atoms is a bridging O atom between two Si atoms while the two other O atoms interact with metals or cations. In the case of spodumene, $LiAl(SiO_3)_2$, the space between the chains is filled by Al atoms and Li$^+$ cations, which both have distorted octahedral coordination (Fig. 1). The structure of α-spodumene (the monoclinic phase) was determined in space group $C2$ by Clark *et al.* (1969) and later by Cameron *et al.* (1973) in the centrosymmetric space group $C2/c$. Clark *et al.* (1969) observed up to ten weak $h0l$ reflections with $l = 2n + 1$ violating the c-glide symmetry; these were not present in the precession photographs of Cameron *et al.* (1973). Graham (1975) showed that structure refinements in the space groups $C2$ or Cc do not modify the centrosymmetric positions of the atoms. Graham also tested the centrosymmetry of the α-spodumene structure by optical methods and argued that the forbidden observations are artefacts owing to the presence of a second phase (tetragonal β-spodumene or hexagonal γ-spodumene). The asymmetric unit of α-spodumene in the space group $C2/c$ contains one half of the chemical formula $LiAl(SiO_3)_2$ with Li$^+$ and Al on special positions (0, y, 1/4).

Compared with our previous studies of the natural zeolites natrolite, $Na_2Al_2Si_3O_{10}.2H_2O$, (Ghermani *et al.*, 1996) and scolecite, $CaAl_2Si_3O_{10}.3H_2O$, (Kuntzinger *et*

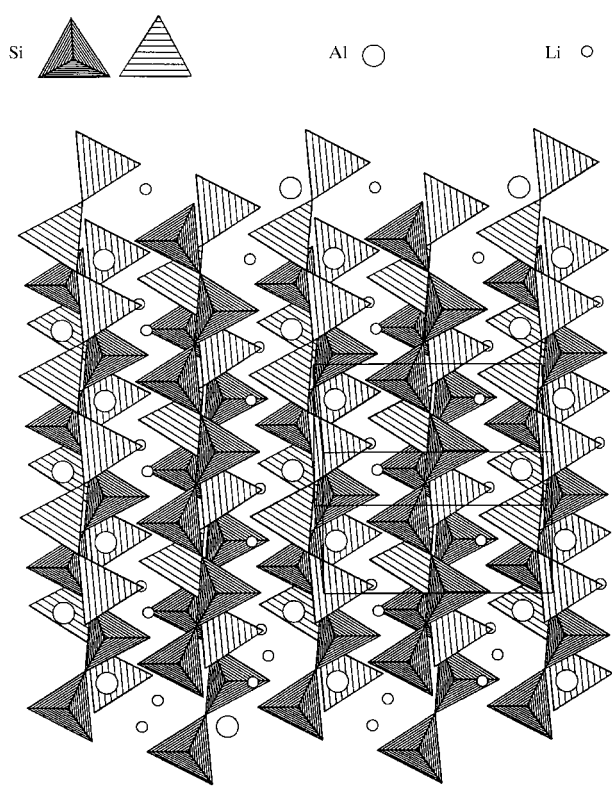

Fig. 1. A view of the structure of α-spodumene projected on the **bc** plane (*STRUPLO*90; Fischer *et al.*, 1991).

al., 1998), which both belong to the tectosilicate group and display connected Si and Al tetrahedra in helicoidal chains, the study of spodumene should provide an insight into the charge density of the Al octahedra in aluminosilicate materials. Furthermore, we are interested in the $Li^+\cdots O$ interaction since cation exchange in industrial zeolites with faujasite-type structures (see, for example, Preuss *et al.*, 1985) makes the lithium-containing compounds more efficient in the adsorption process. In the present study, the charge-density distribution in α-spodumene was derived from room-temperature high-resolution X-ray diffraction data. The experimental electron densities derived from Mo *Kα*- and Ag *Kα*-radiation diffraction data are compared. The shorter X-ray wavelength is generally preferred for materials in which absorption and extinction of the incident beam are important (see, for example, the comparison for forsterite, Mg_2SiO_4, by van der Wal *et al.*, 1987). The Madelung potential at the atomic sites and the electrostatic energy in spodumene are evaluated using the atomic net charges derived from the two data sets.

2. Experimental and methods

2.1. *Data collection and processing*

A good quality nearly parallelepipedic crystal was cut from a large natural specimen of spodumene originating from Afghanistan. The sample used in both X-ray diffraction experiments displayed four cleavage faces (110) and $(1\bar{1}0)$, the other sectioned faces being parallel to $(4\bar{8}\bar{7})$ and $(4\bar{8}\bar{7})$. The face indices were determined using the *MICROS-MICROR* program of the *CAD-4 Diffractometer Software* package (Enraf–Nonius, 1989). Details of the diffraction experiments using Mo *Kα* and Ag *Kα* radiation are given in Table 1. The lattice parameters obtained in this study (Table 1) are slightly different from those of the powder diffraction data of Clark *et al.* (1969) [a = 9.449 (3), b = 8.386 (1), c = 5.215 (2) Å, β = 110.10 (2)°]. Data were collected to resolutions s_{max} (where $s = \sin\theta/\lambda$) = 1.22 $Å^{-1}$ for Mo *Kα* radiation and 1.26 $Å^{-1}$ for Ag *Kα* radiation. Additional azimuthal ψ-offset reflections were collected for both radiations in the complete reciprocal sphere up to a resolution of s = 0.5 $Å^{-1}$ in order to improve the absorption correction. The total X-ray exposure time of the crystal was 298 and 430 h for Mo *Kα* and Ag *Kα*, respectively.

The *DREADD* program package of Blessing (1987, 1989) was used for the data reduction and error analysis. For both data sets, a Lorentzian peak-width variation model was used to integrate the intensity profiles. The instrumental instability coefficients p (McCandlish *et al.*, 1975) based on the statistics of the standard-reflection intensity variations were found to be 0.0130 (2) for Mo *Kα* radiation and 0.0160 (3) for Ag *Kα* radiation. These coefficients were used in the estimation of the variance of each intensity as $\sigma^2(|F_o|^2) = [\sigma_c^2(|F_o|^2) + (p|F_o|^2)^2]$ where F_o is the observed structure factor and σ_c^2 is calculated using the propagation of error based on counting statistics and scan-angle uncertainty. The absorption correction for both data sets was performed using Gaussian numerical integration in the program *ABSORB* (DeTitta, 1985). In addition, the spherical-harmonics empirical correction of Blessing (1995) was also applied. This correction also takes into account an eventual inhomogeneity of the incident X-ray beam. In agreement with Clark *et al.* (1969), space-group forbidden reflections were observed; the most significant intensities [$I > 3\sigma(I)$] were those of $(\bar{2}01)$ and (001) for Ag *Kα* radiation, and (203) and (001) for Mo *Kα* radiation. According to Graham (1975), these reflections were not used in the refinements. The merging and averaging were performed in the Laue group 2/m. The internal-agreement indices reported in Table 1 for the two radiations are quite similar.

2.2. *Multipole refinements*

Conventional and multipole refinements were performed using the least-squares program *MOLLY* (Hansen & Coppens, 1978). The form factors of the core and valence shells of neutral Si, Al and O atoms and the Li^+ cation were calculated from Hartree–Fock wave functions (Clementi & Roetti, 1974). The anomalous-dispersion coefficients were taken from *International Tables for Crystallography* (1995, Vol. C). A description of the multipole model and the refinement strategies have been reported previously in the studies of natrolite (Ghermani *et al.*, 1996) and scolecite (Kuntzinger *et al.*, 1998). The kappa model (Coppens *et al.*, 1979) was used to determine the net atomic charges.

The multipole refinements were performed with multipole expansions in local atomic frames up to hexadecapoles for Si and Al, and up to octopoles for the O atoms. The radial functions of Si and Al atoms were [n_l = 4,4,4,4 (l = 1 to 4)]; ζ's were taken from Clementi & Raimondi (1963): ζ_{Si} = 3.05, ζ_{Al} = 2.72 $bohr^{-1}$ (1 bohr = 0.529 Å). For the O atoms ζ_O = 4.50 $bohr^{-1}$ and the multipole exponents were n_l = 2,2,3 (l = 1 to 3). The twofold-axis local symmetry was imposed on the Al multipole expansion (Kurki-Suonio, 1977). The Li was considered as a cation with a valence charge equal to +1. In all the refinements the unit cell was constrained to be neutral. The best correction for isotropic extinction was obtained with an extinction of type I and a Lorentzian mosaic distribution for the two wavelengths (Becker & Coppens, 1974). The intensity of the most affected reflection $(\bar{2}21)$ was corrected by a factor y = 0.58 for Mo *Kα* and y = 0.68 for Ag *Kα*, corresponding to 42 and 32% extinction, respectively.

A comparison of the final residual indices is given in Table 2. The atomic fractional coordinates and the

Table 1. *Experimental details*

The internal-agreement factors are defined as $R_1 = \sum_{\mathbf{H}} |I(\mathbf{H}) - <I(\mathbf{H})>| / \sum_{\mathbf{H}} |I(\mathbf{H})|$, $R_2 = \{\sum_{\mathbf{H}}[I(\mathbf{H}) - <I(\mathbf{H})>]^2 / \sum_{\mathbf{H}}[I(\mathbf{H})]^2\}^{1/2}$, $wR = \{\sum_{\mathbf{H}} w[I(\mathbf{H}) - <I(\mathbf{H})>]^2 / \sum_{\mathbf{H}} w[I(\mathbf{H})]^2\}^{1/2}$ and $S = \{(M/M-N)\sum_{\mathbf{H}} w[(I(\mathbf{H}) - <I(\mathbf{H})>)/\sigma]^2 / \sum_{\mathbf{H}} w\}^{1/2}$; the intensity $I(\mathbf{H}) = K^{-2}|F_o(\mathbf{H})|^2$ where $|F_o(\mathbf{H})|$ is the modulus of the observed structure factor and K^{-1} is the structure-factor scale factor, M and N are the number of reflections and the number of unique reflections, respectively, and $w = 1/\sigma^2[I(\mathbf{H})]$ is the statistical weight related to the standard uncertainty of the intensity.

	Mo $K\alpha$	Ag $K\alpha$
Crystal data		
Chemical formula	$LiAl(SiO_3)_2$	$LiAl(SiO_3)_2$
Chemical formula weight	186.09	186.09
Cell setting	Monoclinic	Monoclinic
Space group	$C2/c$	$C2/c$
a (Å)	9.462 (1)	9.456 (1)
b (Å)	8.392 (1)	8.386 (1)
c (Å)	5.221 (1)	5.216 (1)
β (°)	110.18 (1)	110.13 (1)
V (Å^3)	389.12 (8)	388.36 (9)
Z	4	4
D_x (Mg m^{-3})	3.18	3.18
Wavelength (Å)	0.7107	0.5608
No. of reflections for cell parameters	25	25
θ range (°)	16.4–30.5	9.4–23.6
μ (mm^{-1})	1.05	0.54
Temperature (K)	293	293
Crystal form	Parallelepiped	Parallelepiped
Crystal size (mm)	0.36 × 0.18 × 0.06	0.36 × 0.18 × 0.06
Crystal colour	Colourless	Colourless
Data collection		
Diffractometer	Enraf–Nonius CAD-4	Enraf–Nonius CAD-4
Data collection method	$\omega/2\theta$ scans	$\omega/2\theta$ scans
Scan speed (° min^{-1})	0.7–4	0.6–4
ω-scan angle (°)	1.0 + 0.35tan θ	1.0 + 0.45tan θ
Absorption correction	Gaussian quadrature (DeTitta, 1985) followed by empirical (Blessing, 1995)	Gaussian quadrature (DeTitta, 1985) followed by empirical (Blessing, 1995)
T_{min}	0.68	0.82
T_{max}	0.95	0.97
No. of measured reflections	12 984	15 850
No. of independent reflections	2945	3241
No. of observed reflections	2366	2261
Criterion for observed reflections	$I > 3\sigma(I)$	$I > 3\sigma(I)$
R_1	0.021	0.021
R_2	0.033	0.028
wR	0.021	0.025
S	0.90	0.88
θ_{max} (°)	60.12	45
Range of h, k, l	$-22 \rightarrow h \rightarrow 22$ $-18 \rightarrow k \rightarrow 20$ $-12 \rightarrow l \rightarrow 11$	$-23 \rightarrow h \rightarrow 23$ $-21 \rightarrow k \rightarrow 21$ $-13 \rightarrow l \rightarrow 13$
No. of standard reflections	3	4
Frequency of standard reflections	Every 120 min	Every 120 min
Intensity decay (%)	0	0
Refinement (see also Table 2)		
Refinement on	F	F
Weighting scheme	$w = 1/[\sigma^2(F^2) + (0.0130F^2)^2]$	$w = 1/[\sigma^2(F^2) + (0.0160F^2)^2]$
$(\Delta/\sigma)_{max}$	0	0
$\Delta\rho_{max}$ (e Å^{-3})	0.3	0.2
$\Delta\rho_{min}$ (e Å^{-3})	−0.1	−0.1
Extinction method	Becker–Coppens type I Lorentzian isotropic	Becker–Coppens type I Lorentzian isotropic
Extinction coefficient	5.0×10^2	4.9×10^2
Source of atomic scattering factors	*International Tables for Crystallography* (1992, Vol. C, Tables 4.2.6.8 and 6.1.1.4)	*International Tables for Crystallography* (1992, Vol. C, Tables 4.2.6.8 and 6.1.1.4)
Computer programs		
Data collection and cell refinement	*CAD*-4 *Diffractometer Software* (Enraf–Nonius, 1989)	*CAD*-4 *Diffractometer Software* (Enraf–Nonius, 1989)
Structure refinement	*MOLLY* (Hansen & Coppens, 1978)	*MOLLY* (Hansen & Coppens, 1978)

Table 2. *Least-squares statistical factors R, wR and GOF for the different refinements for the Mo Kα (1, 2, 3) and Ag Kα (1′, 2′, 3′) data sets*

$s = \sin\theta/\lambda$, $R(F) = \sum |(K^{-1}|F_o| - |F_c|)| / \sum K^{-1}|F_o|$, $wR(F) = [\sum w(K^{-1}|F_o| - |F_c|)^2 / \sum wK^{-2}|F_o|^2]^{1/2}$ and GOF = $[\sum w(K^{-1}|F_o| - |F_c|)^2/m - n]^{1/2}$, where $|F_o|$ and $|F_c|$ are the moduli of the observed and the calculated structure factor, respectively, w is the statistical weight, K^{-1} is the scale factor, n is the number of refined parameters and m is the number of data.

Refinement	s (Å^{-1})	R (%)	wR (%)	GOF	n	m	Type of refinement
Mo $K\alpha$							
1	$0.0 \le s \le 1.22$	1.72	2.60	1.69	2†	2366	Spherical (IAM)
2	$0.0 \le s \le 1.22$	1.37	1.45	0.97	138	2366	Multipolar
3	$0.0 \le s \le 1.22$	1.58	1.85	1.21	12	2366	Kappa
Ag $K\alpha$							
1′	$0.0 \le s \le 1.26$	1.92	2.69	1.45	2†	2261	Spherical (IAM)
2′	$0.0 \le s \le 1.26$	1.55	1.51	0.84	138	2261	Multipolar
3′	$0.0 \le s \le 1.26$	1.77	1.94	1.05	12	2261	Kappa

† Scale factor and extinction parameter after high-order ($s \ge 0.9$ Å^{-1}) refinement of x, y, z and U^{ij}'s.

anisotropic displacement parameters derived from the two data sets by multipole refinement (refinements 2 and 2′ in Table 2) are reported in Table 3. We note that the latter parameters are systematically higher for Ag $K\alpha$ than for Mo $K\alpha$. The same remark holds for the recent two-radiation study of ammonium bis-μ-oxalato-titanate(III) dihydrate, $NH_4[Ti(C_2O_4)_2].2H_2O$, reported by Sheu *et al.* (1996). Multipole parameters of the electron-density model (refinements 2 and 2′) from the two data sets have been deposited.† Fig. 2 displays the residual electron density maps after the multipole refinements. The experimental errors in the electron density are estimated (Cruickshank, 1949; Rees, 1976) by

$$<\sigma^2(\Delta\rho)>^{1/2} = (2/V_{\rm cell})\left\{\sum_H \sigma^2[K^{-1}|F_{\rm obs}(H)|]\right\}^{1/2}$$

to be 0.047 (Mo $K\alpha$) and 0.057 e Å^{-3} (Ag $K\alpha$), and by

$$<\sigma^2_{\rm res}>^{1/2} = (2/V_{\rm cell})\left\{\sum_H [K^{-1}|F_{\rm obs}(H)| - |F_{\rm calc}(H)|]^2\right\}^{1/2}$$

to be 0.062 (Mo $K\alpha$) and 0.057 e Å^{-3} (Ag $K\alpha$), where $V_{\rm cell}$ is the unit-cell volume and K is the scale factor of the diffraction intensity amplitudes $F(H)$.

2.3. *Madelung potential*

The electrostatic potential in the crystal can be derived from the Bragg diffraction data either by Fourier analysis (Stewart, 1979, 1982; Spackman & Stewart, 1981) or by direct calculation using the fitted multipole parameters (Ghermani *et al.*, 1992, 1993). However, the multipole-model parameters cannot be used directly in simulation programs which need net charge sets $\{q_i\}$ in order to estimate the electrostatic part

$$E_{\rm el} = (1/2) \sum_i^{\rm lattice} \sum_j^{\rm cell} q_i q_j / |\mathbf{R}_{ij}|$$

of the total energy of a system. For instance, experimental and formal charge sets have been used by Parker *et al.* (1984) for structure prediction in several types of silicate minerals. For our part, we have used the net atomic charges (as point charges) derived from kappa refinements to calculate the electrostatic (Madelung) potential in spodumene. This physical property at a point **r** in the unit cell is estimated by

$$V(\mathbf{r}) = \sum_l^{\rm lattice} \sum_j^{\rm cell} q_j / |\mathbf{r} - (\mathbf{R}_j + \mathbf{X}_l)|,$$

where q_j is the net charge of the atom j at $\mathbf{R}_j$, and $\mathbf{X}_l$ are the translation vectors of the direct crystal lattice.

We have modified the computer program *ELECTROS* (Ghermani *et al.*, 1992) in order to calculate and map out the electrostatic potential. In these calculations, the crystal is constructed by the superposition of shells of unit cells. The neutrality of the unit cell and its zero dipole moment owing to the inversion symmetry in α-spodumene satisfy the criterion of a rapid convergence of such R^{-n} lattice sums (see, for example, Williams, 1989). The sum given above is formally extended to infinity, which means that the values of the potential correspond to an infinite crystal of spodumene. In fact, we found that convergence is already reached for distances of three to five times the unit-cell dimensions. On the other hand, in order to obtain the Coulomb potential on an absolute scale, we have taken the value of the mean inner potential Φ_0 into account in the calculation of the electrostatic potential. Initially, this quantity was evaluated theoretically for electron

† Supplementary data for this paper are available from the IUCr electronic archives (Reference: SH0121). Services for accessing these data are described at the back of the journal.

microscopy by Bethe (1928), who showed that the mean inner potential is related to the quadrupolar moment of the unit cell. Spackman & Stewart (Spackman & Stewart, 1981; Stewart, 1982) were the first crystallographers to apply the pro-crystal mean inner potential in the calculation of the electrostatic potential in crystals based on the independent atom model (IAM) according to $\Phi_0^{\text{pro-crystal}} = -(2\pi/3V_{\text{cell}}) \int_{\text{cell}} r^2 \rho_{\text{IAM}}(r) d^3r$. Becker & Coppens (1990) have estimated Φ_0 for an infinite crystal with respect to multipole parameters of the Hansen–Coppens electron density pseudo-atom model (Hansen & Coppens, 1978). Recently, O'Keeffe & Spence (1994) suggested the use, if available, of the experimental value of the mean inner potential from electronic holograms (Gajdardziska-Josifovska *et al.*, 1993) rather than the calculated one. They also have shown that the pro-crystal evaluation overestimates Φ_0 relative to the experiment and that the pseudo-atom model estimation does not take into account the surface contribution, which does not appear to be negligible for a finite crystal. However, this problem cancels for non-overlapping pseudo-atoms in the unit cell, such as point charges (O'Keeffe & Spence, 1994). Accordingly, we have estimated the mean inner potential for an infinite crystal of spodumene by the Becker–Coppens (1990) relation $\Phi_0 = -(2\pi/3V_{\text{cell}}) \sum_j^{\text{cell}} q_j R_j^2$.

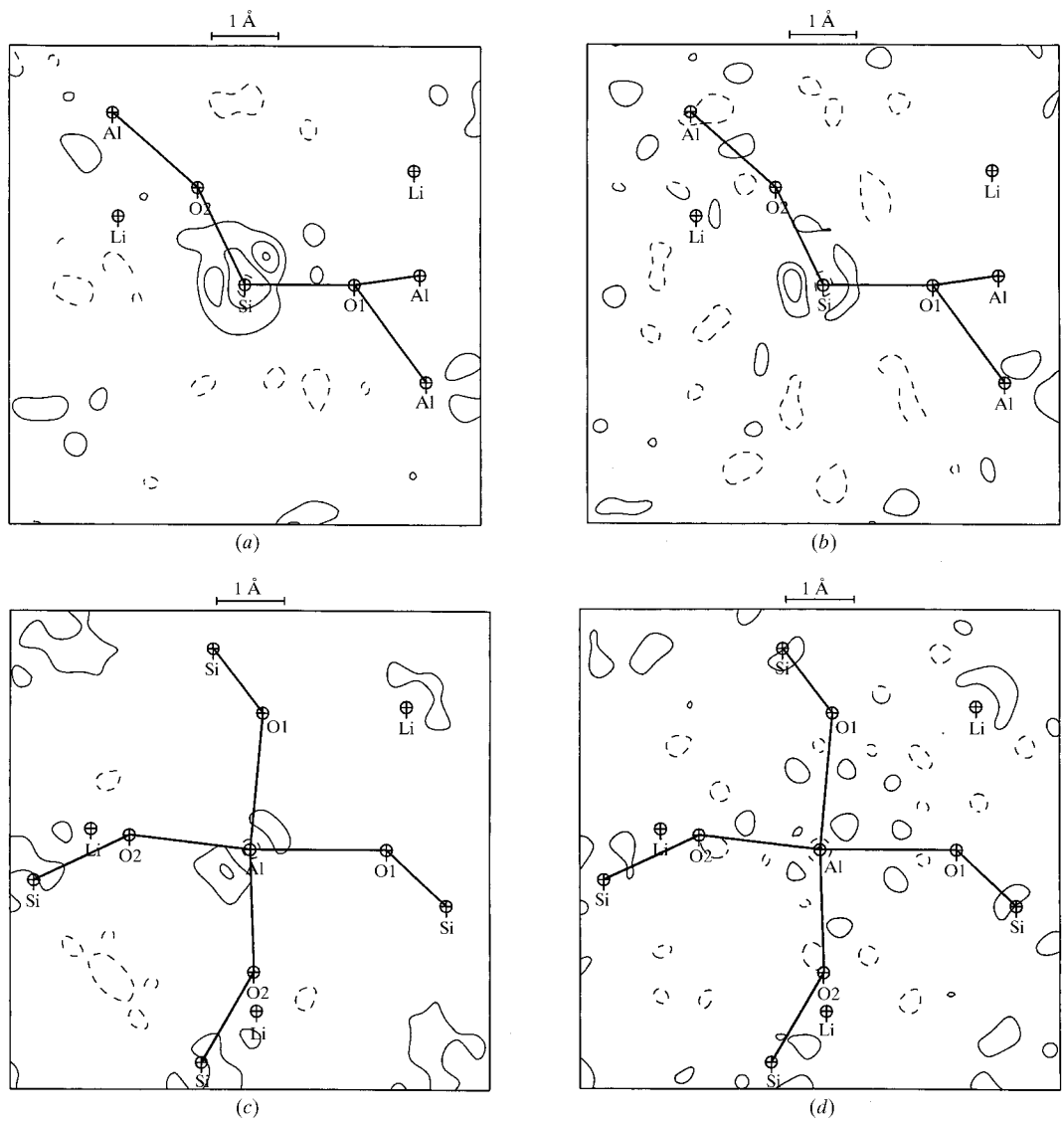

Fig. 2. Residual electron densities in the O—Si—O [(*a*) Mo $K\alpha$; (*b*)Ag $K\alpha$] and O—Al—O [(*c*) Mo $K\alpha$; (*d*) Ag $K\alpha$] planes in spodumene after the multipole refinements of the two data sets. Contour intervals are 0.1 e Å^{-3}, negative contours are dashed and the zero contour is omitted. (Fourier summation over data with $0 \leq s \leq 0.9$ Å^{-1}.)

Table 3. *Atomic fractional coordinates, equivalent isotropic displacement amplitudes U_{eq} ($Å^2$) and anisotropic displacement amplitudes U^{ij} ($Å^2$) × 10^5 after multipole refinements 2 and 2′ (Table 2)*

For each pair of rows the values in the upper row were obtained using Ag $K\alpha$ radiation and the values in the lower row were obtained using Mo $K\alpha$ radiation. S.u.'s are given in parentheses.

$$U_{\rm eq} = (1/3)\Sigma_i\Sigma_j U^{ij} a^i a^j \mathbf{a}_i.\mathbf{a}_j.$$

	x	y	z	$U_{\rm eq}$
Si	0.29410 (1)	0.09345 (1)	0.25593 (2)	0.00397 (3)
	0.29410 (1)	0.09347 (1)	0.25592 (1)	0.00377 (2)
Al	0	0.90669 (2)	1/4	0.00424 (4)
	0	0.90667 (1)	1/4	0.00409 (2)
O_1	0.10975 (2)	0.08237 (2)	0.14061 (4)	0.00495 (5)
	0.10971 (2)	0.08232 (2)	0.14056 (4)	0.00479 (4)
O_2	0.36470 (3)	0.26708 (3)	0.30050 (5)	0.00771 (6)
	0.36470 (2)	0.26713 (2)	0.30048 (4)	0.00758 (5)
O_3	0.35663 (2)	0.98668 (3)	0.05824 (4)	0.00766 (6)
	0.35663 (2)	0.98674 (3)	0.05827 (4)	0.00749 (5)
Li	0	0.27494 (14)	1/4	0.01474 (4)
	0	0.27467 (13)	1/4	0.01464 (4)

	U^{11}	U^{22}	U^{33}	U^{12}	U^{13}	U^{23}
Si	386 (3)	447 (3)	355 (3)	−62 (2)	125 (2)	−20 (2)
	360 (2)	432 (2)	332 (2)	−61 (2)	109 (2)	−19 (2)
Al	420 (4)	427 (4)	418 (4)	0	134 (3)	0
	407 (3)	419 (3)	393 (3)	0	126 (3)	0
O_1	389 (5)	587 (6)	469 (6)	−33 (5)	96 (4)	20 (5)
	368 (4)	563 (5)	463 (5)	−36 (4)	90 (4)	13 (4)
O_2	817 (7)	569 (6)	991 (7)	−291 (5)	392 (6)	−84 (6)
	799 (6)	560 (5)	983 (6)	−293 (4)	393 (5)	−98 (5)
O_3	590 (6)	1141 (8)	529 (6)	68 (6)	145 (5)	−339 (6)
	572 (5)	1129 (6)	508 (5)	67 (5)	139 (4)	−337 (5)
Li	1536 (45)	1370 (45)	1508 (45)	0	514 (36)	0
	1461 (39)	1388 (40)	1585 (41)	0	577 (32)	0

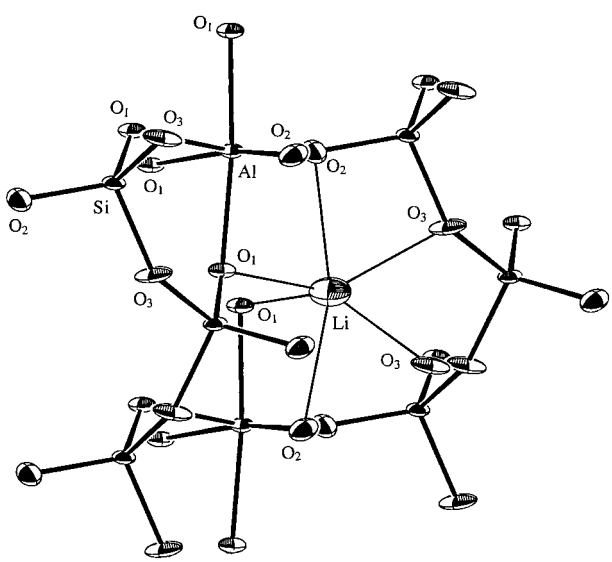

Fig. 3. An *ORTEP*II (Johnson, 1976) view and the atom numbering of the spodumene structure (from the Ag $K\alpha$ multipole refinement, 2′ in Table 2). Displacement ellipsoids are shown at the 50% probability level.

3. Results and discussion

3.1. *Crystal structure of spodumene*

An *ORTEP*II (Johnson, 1976) view of the α-spodumene structure is given in Fig. 3 showing the sixfold coordination of the Al atom and Li^+ cation. The values of the bond lengths and angles obtained after the multipole refinements (2 and 2′ in Table 2) are reported in Table 4. We note that the differences in bond lengths obtained from the two data sets do not exceed 7σ but the angle values are closer. The short Si—O_2 bond length of 1.5866 (2) Å for Mo $K\alpha$ radiation [1.5852 (2) Å for Ag $K\alpha$] also corresponds to the shortest Al—O interatomic distance [Al—O_2 = 1.8200 (2) for Mo $K\alpha$ and 1.8190 (2) Å for Ag $K\alpha$]. All these values are on average in agreement with those reported by Cameron *et al.* (1973). O_3 is the bridging O atom between the Si atoms in the chains. Thus, each Si atom is bonded to two O_3 atoms with distances 1.6242 (2) and 1.6280 (2) Å (Mo $K\alpha$ radiation), and 1.6230 (2) and 1.6268 (2) Å (Ag $K\alpha$ radiation). The Al atom is octahedrally coordinated by four O_1 and two O_2 atoms with bond lengths in the range 1.82 to 1.99 Å. The Li^+ cation is surrounded by two O_1,

Table 4. *Selected bond lengths (Å) and angles (°) in α-spodumene from multipole refinements 2 and 2′ (Table 2)*

S.u.'s are given in parentheses.

	Mo $K\alpha$	Ag $K\alpha$		Mo $K\alpha$	Ag $K\alpha$
$Si-O_2$	1.5866 (2)	1.5852 (2)	$O_2-Si-O_3^{i}$	111.87 (1)	111.89 (1)
$Si-O_3^{i}$	1.6242 (2)	1.6230 (2)	$O_2-Si-O_3^{ii}$	104.11 (1)	104.07 (1)
$Si-O_3^{ii}$	1.6280 (2)	1.6268 (2)	O_2-Si-O_1	116.55 (1)	116.54 (1)
$Si-O_1$	1.6404 (2)	1.6393 (2)	$O_3^{i}-Si-O_3^{ii}$	107.32 (1)	107.32 (1)
			$O_3^{i}-Si-O_1$	108.04 (1)	108.02 (1)
			$O_3^{ii}-Si-O_1$	108.50 (1)	108.55 (1)
$Al-O_2^{iii}$	1.8200 (2)	1.8190 (2)	$O_2^{iii}-Al-O_2^{viii}$	99.90 (1)	99.87 (2)
$Al-O_1^{iv}$	1.9451 (2)	1.9447 (2)	$O_2^{iii}-Al-O_1^{ix}$	88.43 (1)	88.45 (1)
$Al-O_1^{v}$	1.9965 (2)	1.9951 (2)	$O_2^{iii}-Al-O_1^{v}$	167.85 (1)	167.87 (2)
			$O_1^{v}-Al-O_1^{ix}$	84.82 (1)	84.80 (1)
			$O_2^{iii}-Al-O_1^{ii}$	91.52 (1)	91.55 (1)
			$O_2^{iii}-Al-O_1^{iv}$	91.98 (1)	91.94 (1)
			$O_1^{ii}-Al-O_1^{ix}$	78.88 (1)	78.93 (1)
			$O_1^{ii}-Al-O_1^{v}$	97.05 (1)	97.02 (1)
			$O_1^{iv}-Al-O_1^{ii}$	174.55 (1)	174.59 (1)
$Li-O_1$	2.1021 (8)	2.1019 (9)	$O_1-Li-O_1^{x}$	79.67 (4)	79.60 (4)
$Li-O_3^{vi}$	2.2524 (9)	2.2491 (9)	$O_2^{vii}-Li-O_2^{xi}$	162.29 (5)	162.21 (6)
$Li-O_2^{vii}$	2.2797 (3)	2.2791 (3)	$O_3^{vi}-Li-O_3^{xii}$	75.59 (3)	75.72 (3)
			$O_1-Li-O_3^{xii}$	116.70 (1)	116.68 (1)
			$O_1-Li-O_3^{vi}$	139.84 (1)	139.84 (1)
			$O_2^{xi}-Li-O_1$	75.92 (2)	75.92 (2)
			$O_2^{vii}-Li-O_1$	90.40 (3)	90.32 (3)
			$O_3^{xii}-Li-O_2^{vii}$	68.03 (1)	68.00 (1)
			$O_3^{xii}-Li-O_2^{xi}$	128.13 (4)	128.22 (4)
$Si-O_1-Al^{iv}$	119.85 (1)	119.90 (1)	$Si-O_1-Li$	114.76 (2)	114.76 (2)
$Si-O_1-Al^{i}$	121.95 (1)	121.93 (1)	$Si-O_2-Li^{vii}$	93.91 (3)	93.89 (3)
$Si-O_2-Al^{xiii}$	148.37 (1)	148.39 (2)	$Si^{v}-O_3-Li^{xv}$	116.68 (1)	116.65 (1)
$Si^{v}-O_3-Si^{xiv}$	138.91 (1)	138.89 (2)	$Si^{xiv}-O_3-Li^{xv}$	93.78 (2)	93.86 (2)
$Al^{iv}-O_1-Al^{i}$	101.12 (1)	101.07 (1)	$Al^{iv}-O_1-Li$	96.51 (1)	96.48 (1)
			$Al^{i}-O_1-Li$	97.76 (2)	97.81 (2)
			$Al^{xiii}-O_2-Li^{vii}$	94.29 (2)	94.28 (2)

Symmetry codes: (i) $x, y-1, z$; (ii) $x, 1-y, \frac{1}{2}+z$; (iii) $x-\frac{1}{2}, \frac{1}{2}+y, z$; (iv) $-x, 1-y, -z$; (v) $x, 1+y, z$; (vi) $x-\frac{1}{2}, y-\frac{1}{2}, z$; (vii) $\frac{1}{2}-x, \frac{1}{2}-y, 1-z$; (viii) $\frac{1}{2}-x, \frac{1}{2}+y, \frac{1}{2}-z$; (ix) $-x, 1+y, \frac{1}{2}-z$; (x) $-x, y, \frac{1}{2}-z$; (xi) $x-\frac{1}{2}, \frac{1}{2}-y, z-\frac{1}{2}$; (xii) $\frac{1}{2}-x, y-\frac{1}{2}, \frac{1}{2}-z$; (xiii) $\frac{1}{2}+x, y-\frac{1}{2}, z$; (xiv) $x, 1-y, z-\frac{1}{2}$; (xv) $\frac{1}{2}+x, \frac{1}{2}+y, z$.

two O_2 and two O_3 atoms with bond lengths in the range 2.10 to 2.28 Å. These interatomic distances are slightly longer than those reported for Li^+-O [2.087 (1) to 2.189 (1) Å] in $LiFePO_4$ by Streltsov *et al.* (1993) where Li^+ is also octahedrally coordinated.

3.2. *Electron deformation density maps*

The spodumene structure contains $Si-O_3-Si$ and $Si-O_2-Al$ bridges interacting with the Li^+ cations. The main difference with respect to our previous studies of natrolite, $Na_2Al_2Si_3O_{10}.2H_2O$, (Ghermani *et al.* 1996) and scolecite, $CaAl_2Si_3O_{10}.3H_2O$, (Kuntzinger *et al.*, 1998) is that the Al atom has octahedral coordination. The deformation electron density features revealed by the Mo $K\alpha$ and Ag $K\alpha$ data sets are globally very similar. Furthermore, a good agreement between the experimental, the dynamic (see supplementary material†) and the static electron density maps is noted.

There are three $Si-O-Al$ bridges involving O_1 and O_2 in spodumene, one $Si-O-Si$ bridge involving the silicate-chain O atom O_3, and one $Al-O-Al$ bridge involving O_1. Fig. 4 compares the $Si-O-Al$ static deformation electron density maps obtained after the multipole refinements with Mo $K\alpha$ (Fig. 4*a*) and Ag $K\alpha$ (Fig. 4*b*) data. In the study of scolecite (Kuntzinger *et al.*, 1998) we emphasized the correlation between the electron density and the geometrical features (large angles imply short interatomic distances) on the one hand and the chemical environment (presence of cations) on the other. In the case of the $Si-O_1-Al$ bridge in spodumene [$Si-O_1-Al(-x, 1-y, -z)$ 119.85 (1) and $Si-O_1-Al(x, y-1, z)$ 121.95 (1)° (Mo $K\alpha$)], the polarization of the O_1 electron density towards the other Al atom [$O_1-Al(-x, 1-y, -z)$ 1.9451 (2), $O_1-Al(x, y-1, z)$ 1.9965 (2) Å] and the Li^+ cation [O_1-Li^+ 2.1021 (8) Å] is more pronounced than for $Si-O_2-Al$ [$Si-O_2-Al(\frac{1}{2}+x, -\frac{1}{2}+y, z)$ 148.37 (1)°] where O_2 is linked to only one Li^+ cation [$O_2-Li^+(\frac{1}{2}-x, \frac{1}{2}-y, 1-$

† See deposition footnote on p. 276.

z) 2.2797 (3) Å]. The average value of the electron-peak heights in Si—O [Si—O_1 1.6404 (2) and Si—O_2 1.5866 (2) Å (Mo $K\alpha$)] is 0.45 e $Å^{-3}$ in the two Si—O—Al bridges compared to 1.0 e $Å^{-3}$ found in scolecite, in which Al has tetrahedral coordination and the Si—O interatomic distances are 1.6008 (8) and 1.6127 (7) Å.

In the Al—O bonds, the electron density is clearly concentrated towards the O atoms compared with the more evenly shared electron density in the Si—O bonds. However, the charge density is slightly diluted in Al—O_2 where the bond is short [O_2—Al($-\frac{1}{2}+x$, $\frac{1}{2}+y$, z) 1.8200 (2) Å]. The electron-peak heights in the Al—O bonds are 0.3 (Mo $K\alpha$) and 0.4 e $Å^{-3}$ (Ag $K\alpha$) in Si—O_1—Al bridges and 0.4 (Mo $K\alpha$) and 0.5 e $Å^{-3}$ (Ag $K\alpha$) in Si—O_2—Al. This is in excellent agreement with the recent results of Graafsma *et al.* (1998) in Al_2O_3 where Al is hexacoordinate and the Al—O interatomic distances are 1.849 and 1.966 Å.

In Fig. 5, the electron density concentration around the O atom and the polarization towards the Li^+ cation

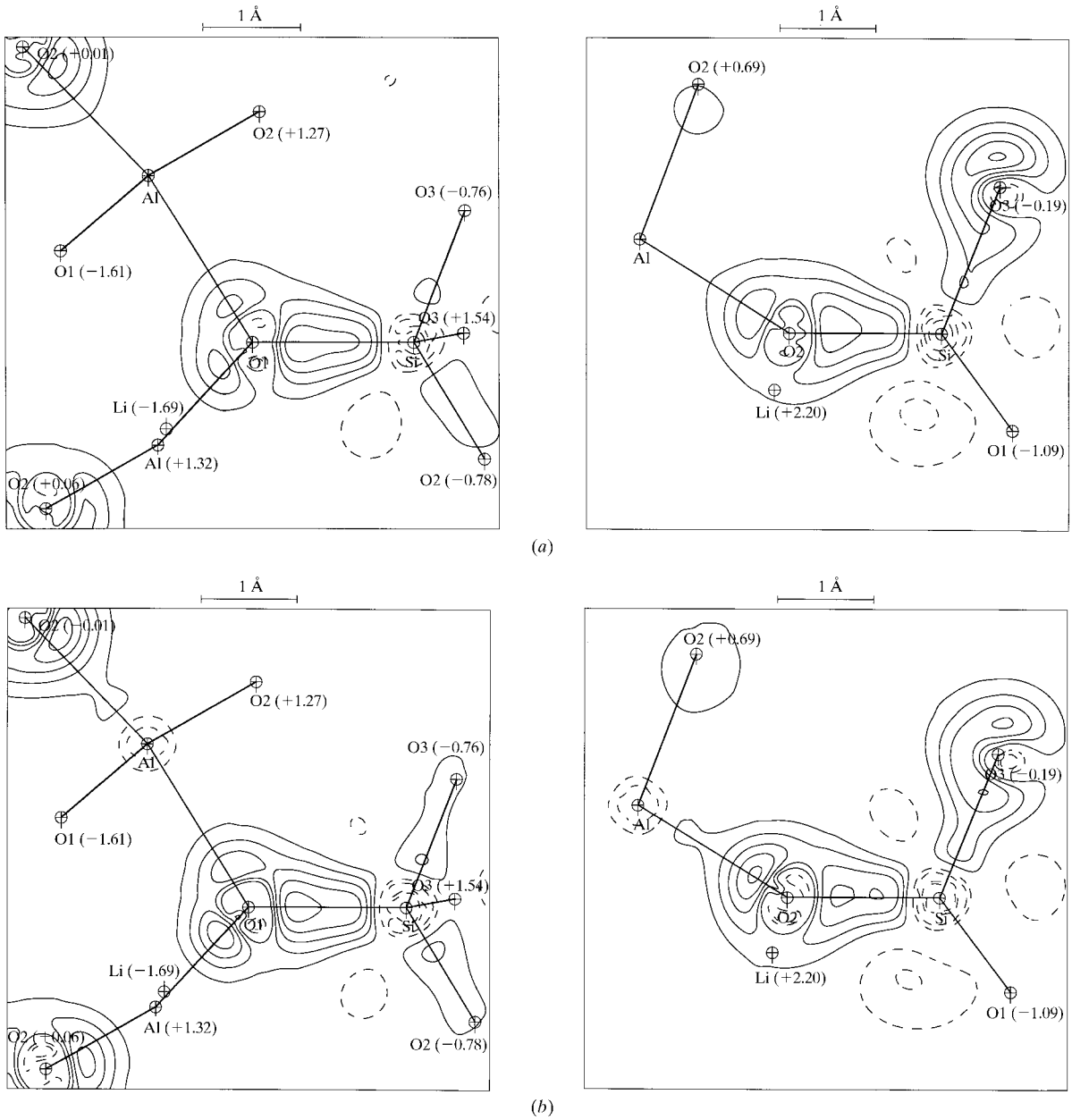

Fig. 4. The static deformation electron density in the Al—O—Si bridge planes. (*a*) Al—O_1—Si and Al—O_2—Si from Mo $K\alpha$ data. (*b*) Al—O_1—Si and Al—O_2—Si from Ag $K\alpha$ data. Contours are as in Fig. 2. The distances to the planes for the out-of-plane atoms are indicated in parentheses.

Table 5. *Results of the kappa refinements (3 and 3′ in Table 2) for the two data sets*

For each pair of rows the values in the upper row were obtained using Ag $K\alpha$ radiation and the values in the lower row were obtained using Mo $K\alpha$ radiation. S.u.'s are given in parentheses. The s.u.'s of the differences of the net atomic charges are calculated as the root-mean squares of the sum of the corresponding variances.

	κ	Atomic charge	Differences of atomic charges
Si	1.18 (2)	1.86 (6)	
	1.13 (2)	1.73 (6)	−0.13 (9)
Al	1.37 (5)	1.94 (4)	
	1.10 (4)	1.54 (5)	−0.40 (7)
O_1	0.944 (2)	−1.10 (4)	
	0.950 (2)	−0.95 (4)	+0.15 (6)
O_2	0.942 (3)	−1.13 (4)	
	0.949 (2)	−1.01 (4)	+0.12 (6)
O_3	0.949 (3)	−1.10 (4)	
	0.952 (2)	−1.04 (4)	+0.06 (6)
Li	1.00	+1.00	
	1.00	+1.00	

are also seen in the Si—O_3—Si bridge [Si(x, $y+1$, z)—O_3—Si(x, $1-y$, $-\frac{1}{2}+z$) 138.91 (1)°, Si—O_3(x, $-1+y$, z) 1.6242 (2) and Si—O_3(x, $1-y$, $\frac{1}{2}+z$) 1.6280 (2) Å (Mo $K\alpha$)]. The shift of the electron density towards the interior of the Si—O—Si angle, as reported in silicates (Gibbs *et al.*, 1997) and aluminosilicates (Kuntzinger *et al.*, 1998), is also observed in spodumene. In the plane of the Si—O—Si bridge, the electron density peaks are 0.4 Å from the Si atom and their heights reach 0.4 to 0.5 e Å^{-3}. These features compare well qualitatively with those reported for scolecite (Kuntzinger *et al.*, 1998) but the values are somewhat different: in scolecite, the Si—O—Si electron density peaks are in the range 0.6 to 0.9 e Å^{-3} in the aluminosilicate chains.

3.3. *Kappa refinements and atomic net charges*

The kappa refinements (Coppens *et al.*, 1979) were carried out assigning to each atom a variable valence population P_{val} related to the net charge ($q = N_{val} - P_{val}$, where N_{val} is the valence population of the free atom) and a κ parameter taking into account the contraction or expansion of the spherical valence shell. The +1 charge of the Li^+ cation was kept fixed in these refinements. Table 5 lists the κ values and the atomic charges q obtained from the two data sets. The κ value of 1.37 (5) for Al derived from the Ag $K\alpha$ data is significantly larger than the value of 1.10 (4) derived from the Mo $K\alpha$ data. Likewise, the largest discrepancy between the net charges appears for this atom [+1.94 (4) (Ag $K\alpha$) and +1.54 (5) e (Mo $K\alpha$)]. In comparison, the study of topaz, $Al_2[SiO_4]F_2$, (Mo $K\alpha$ data) by Ivanov *et al.* (1998) yielded a charge of +1.53 (12) e and a corresponding κ of 1.04 (4) for an octahedrally coordinated Al atom. These values are in good agreement with those derived from Mo $K\alpha$ data in the title compound. On the other hand, the charges derived earlier from an Mo $K\alpha$ X-ray diffraction experiment on α-spodumene by Sasaki *et al.* (1980) but based on a volume integration method involving the atomic radial electronic distribution are

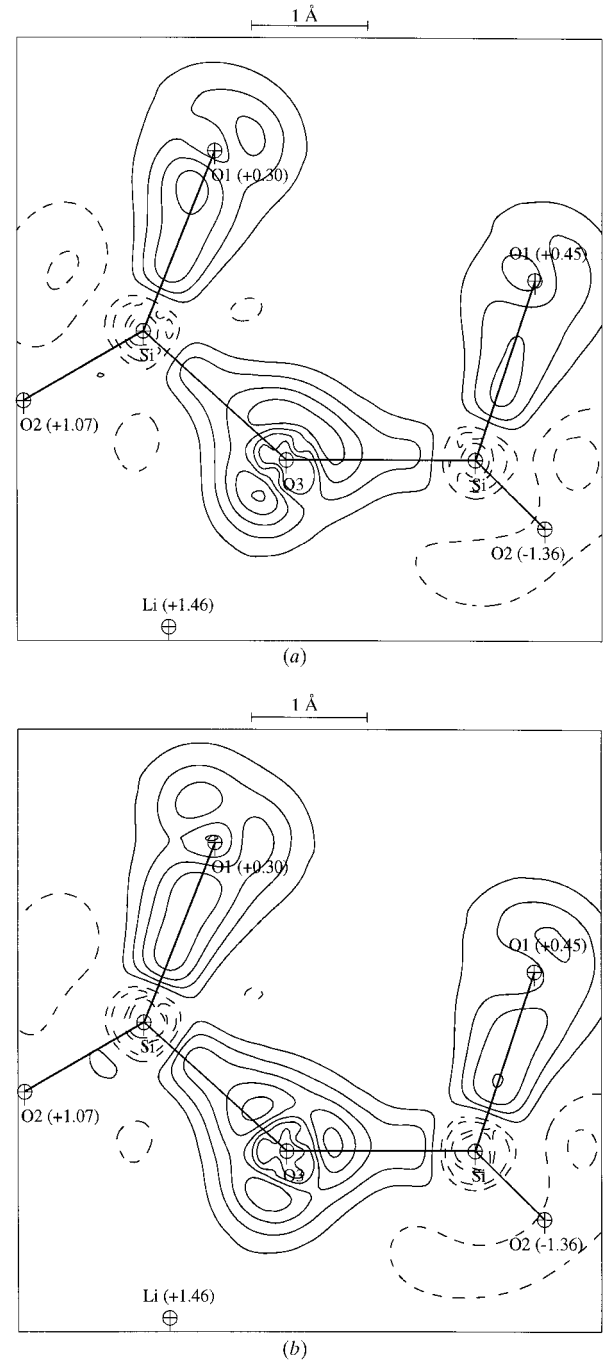

Fig. 5. The static deformation electron density in the Si—O—Si bridge planes. (*a*) Si—O_3—Si from Mo $K\alpha$ data. (*b*) Si—O_3—Si from Ag $K\alpha$ data. Contours are as in Fig. 2. The distances to the planes for the out-of-plane atoms are indicated in parentheses.

quite different from our results: q(Si) = +2.4 (1), q(Al) = +2.4 (1), q(O) = −1.3 to −1.4 and q(Li) = 0.7 (1) e.

In comparison with this study, the two-radiation X-ray study of corundum, Al_2O_3, by Lewis *et al.* (1982) yielded the values κ = 1.09 (5) and q = +1.24 (5) e (Mo $K\alpha$), and κ = 1.20 (6) and q = +1.32 (5) e (Ag $K\alpha$) for the Al atom. More significant differences in the charge and the kappa values were reported for tetrahedrally coordinated Al in natrolite, $Na_2Al_2Si_3O_{10}.2H_2O$, [q(Al) = +1.5 (1) e, κ = 1.10 (2), Mo $K\alpha$ data; Ghermani *et al.*, 1996] and in scolecite, $CaAl_2Si_3O_{10}.3H_2O$, [q(Al) = +1.9 (1) e, κ = 1.5 (1), Ag $K\alpha$ data; Kuntzinger *et al.*, 1998]. For spodumene, we checked that κ(Al) is significantly different from 1.0 using the statistical F-test based on the sums $\sum_H w[K^{-1}|F_{obs}(H)| - |F_{calc}(H)|]^2$ (Prince, 1994). Several refinement strategies have been tested: alternate refinement of P_{val} and κ, or refinement of both parameters. Furthermore, no significant influence of the most extinction-affected reflections on the κ or P_{val} values has been observed. However, the correlation between the kappa parameter and the charge has been clearly shown by Coppens *et al.* (1979). For instance, when we keep the Al κ value fixed at 1.10 in the kappa refinement against Ag $K\alpha$ data, the fitted values of the atomic charges, not only for the Al atom but for all atoms in the asymmetric unit, are very close to those derived from Mo $K\alpha$ data. *Vice versa*, an Al κ value fixed at 1.37 in the Mo $K\alpha$-data kappa refinement yields the charges obtained with the Ag $K\alpha$ data. Although there is an obvious correlation between the fitted values of the P_{val} and κ parameters, only the valence populations were used in the point-charge electrostatic properties calculations.

3.4. *Madelung potential in spodumene*

We have shown (Ghermani *et al.*, 1993) that the main contribution to the electrostatic potential in organic materials comes from the P_{val} parameters related to the net atomic charges. For spodumene we have checked that the electrostatic potential values calculated with all multipole parameters on the one hand and κ, P_{val} parameters obtained after the kappa refinements on the other are almost equal outside spheres of 2 Å radii centred at the nuclei positions. In this way and according to the Gauss theorem, the atomic point charges related to kappa-refinement P_{val}'s can be used to estimate the electrostatic potential in the crystal of spodumene. We have calculated the Madelung potential using the method of lattice summation given in §2.3. The mean inner potential values calculated with the charges from the Mo $K\alpha$ and Ag $K\alpha$ data are Φ_0 = 1.47 and 1.90 e Å^{-1}, respectively (1 e Å^{-1} = 14.4 V and 1 e^2 Å^{-1} = 332.4 kcal mol^{-1} = 1389.4 kJ mol^{-1}). They were used to get the electrostatic potential on an absolute scale and to fulfil the boundary conditions $\int_{cell} V(r)d^3r = 0$ (Stewart, 1982; Spackman & Weber, 1988). The electrostatic potential was calculated in the planes containing the Al atom and the Li^+ cation. In order to display the electrostatic potential basins created by the

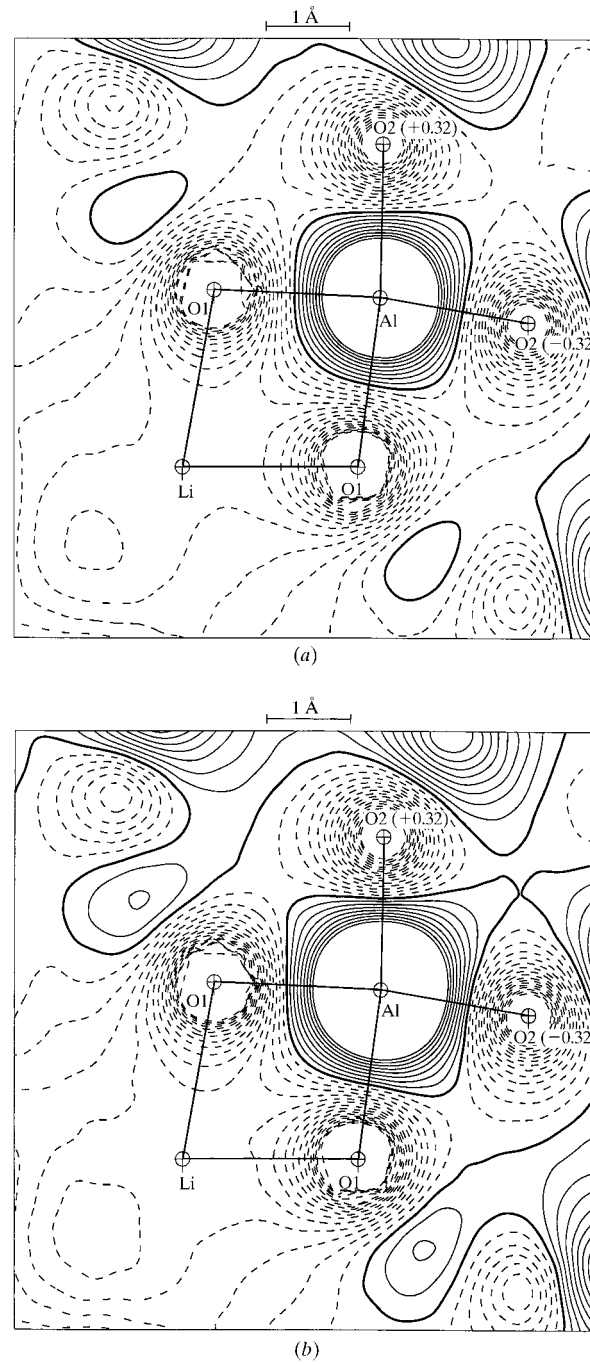

Fig. 6. The electrostatic potential in the $O_1-Li^+-O_1$ plane in spodumene. The Li^+ contribution was omitted from the calculation. (*a*) From the Mo $K\alpha$ data. (*b*) From the Ag $K\alpha$ data. Contour intervals are 0.1 e Å^{-1}, negative contours are dashed and the zero contour is shown as a bold line. The distances to the planes for the out-of-plane atoms are indicated in parentheses.

Table 6. *Madelung potential V (in e Å^{-1}) on the atomic sites in spodumene and electrostatic energy (e^2 Å^{-1}) of the chemical formula LiAl(SiO$_3$)$_2$ derived from the two data sets*

The s.u. of the electrostatic energy for both data sets is about 0.45 e^2 Å^{-1} and was estimated as the root-mean square of the sum of the variances of qV with a crude s.u. value of the experimental potential equal to 0.1 e Å^{-1}.

	Ag $K\alpha$		Mo $K\alpha$	
	V	qV	V	qV
Si	−1.35	−2.51	−1.31	−2.28
Al	−1.19	−2.30	−1.04	−1.60
O_1	+1.47	−1.62	+1.21	−1.15
O_2	+1.40	−1.59	+1.18	−1.19
O_3	+1.38	−1.51	+1.24	−1.29
Li	−0.44	−0.44	−0.52	−0.52
LiAl(SiO$_3$)$_2$		−8.60		−6.97

framework of spodumene, the contributions to the electrostatic potential of the Al atoms and the Li^+ cation were omitted in the calculation. The same method has been used previously in the case of the dehydrated sodium zeolite *A* by Spackman & Weber (1988) and in natrolite (Ghermani *et al.*, 1996).

Fig. 6 shows the electrostatic potential in the plane O_1-Li-O_1. The values of the electrostatic potential around the Li^+ cation site are in the range −0.4 e Å^{-1} (Fig. 6*b*, Ag $K\alpha$) to −0.5 e Å^{-1} (Fig. 6*a*, Mo $K\alpha$). In comparison, we found that the electrostatic potential on the site of the Na^+ cation in NaCl calculated with a fully ionic model (Na^{+1}, Cl^{-1}) is −0.62 e Å^{-1}, which is in excellent agreement with the energetic value of −862.825 kJ mol^{-1} given by Williams (1989). The average value of −0.45 e Å^{-1} at the lithium site in spodumene is in good agreement with the value of −0.48 e Å^{-1} found at one Na^+ cation site in the large cavity of the dehydrated sodium zeolite *A* (Spackman & Weber, 1988). The values of the electrostatic potential obtained by Preuss *et al.* (1985) by a point-charge calculation on the vacant cation site in the large cavities of faujasite-type zeolites (zeolite *X*) reach −10 V (−0.69 e Å^{-1}) for Ca^{2+} and −15 V (−1.04 e Å^{-1}) for La^{3+}. In the channel of the natural zeolite natrolite (Ghermani *et al.*, 1996) the electrostatic potential was found to be −1.5 e Å^{-1}. On the other hand, the features of the electrostatic potential around the Li^+ cation are somewhat different when we consider the topology of this property. The electrostatic potential calculated with the fitted charges (Figs. 6*a* and 6*b*) is flat around the cation, displaying a weak electrostatic field at this site.

The maps in Fig. 7 display the electrostatic potential around the Al-atom site in the plane O_1-Al-O_1. The shape of the electrostatic potential is almost the same for the two sets of charges. The minima of the potential are −1.2 e Å^{-1} for Ag $K\alpha$-derived charges and −1.0 e Å^{-1} for Mo $K\alpha$-derived charges. Table 6 lists the Madelung potential at the atomic sites in spodumene and the related electrostatic energy $(1/2)\sum_j q_j V(\mathbf{R}_j)$ for the chemical formula LiAl(SiO$_3$)$_2$. This latter quantity is 23% lower for the Ag $K\alpha$-derived net charges

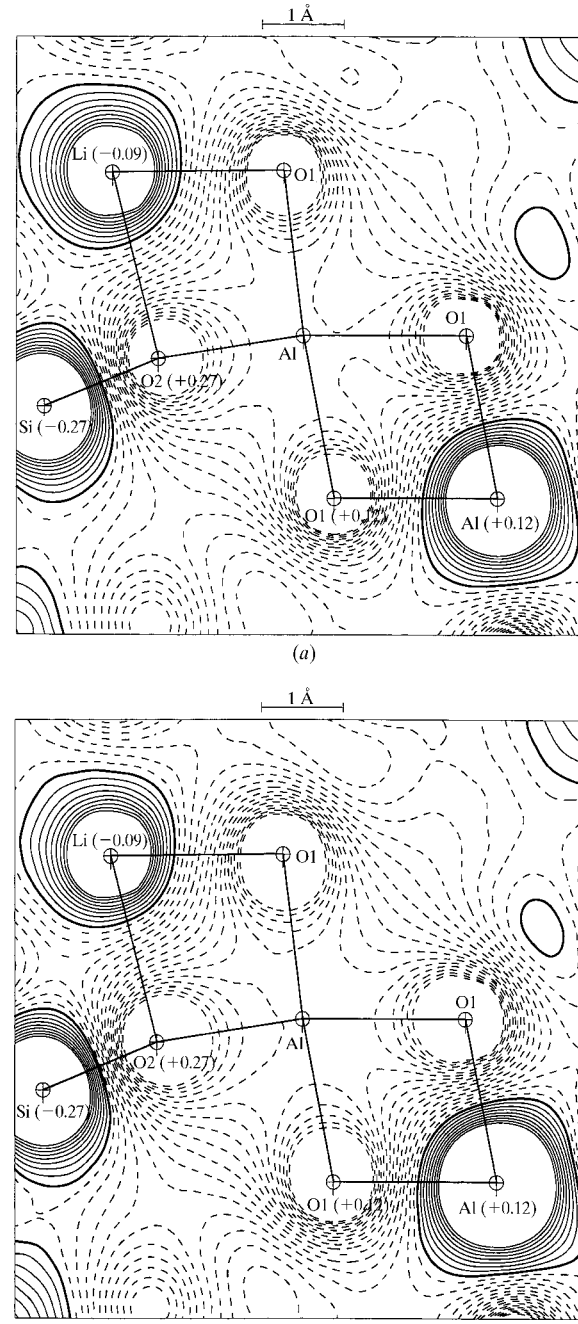

Fig. 7. The electrostatic potential in the O_1-Al-O_1 plane in spodumene. The Al contribution was omitted from the calculation. (*a*) From the Mo $K\alpha$ data. (*b*) From the Ag $K\alpha$ data. Contours are as in Fig. 6. The distances to the planes for the out-of-plane atoms are indicated in parentheses.

(-8.60 e^2 Å^{-1} = -123.84 eV) compared with the Mo$K\alpha$-derived value of -6.97 e^2 Å^{-1} (-100.37 eV). On the other hand, the average values of the Madelung potential calculated with the refined charges at the O-atom sites are 1.43 e Å^{-1} (20.60 V) for the Ag $K\alpha$ data set and 1.21 e Å^{-1} (17.42 V) for the Mo $K\alpha$ data set. These values are in good agreement with the earlier empirical calculations of O'Keeffe (1979), giving a Madelung potential of about 20 V on O-atom sites in different oxides.

4. Concluding remarks

The experimental electron deformation densities obtained from high-resolution Mo $K\alpha$ and Ag $K\alpha$ radiation X-ray diffraction data sets are almost identical in α-spodumene. However, details in the deformation density maps are more pronounced with the shorter wavelength Ag $K\alpha$ radiation. Compared with the features of the electron density in the Al—O bond of a tetrahedrally coordinated Al atom, the shift of the electron density towards the O atoms gives a more ionic character to this bond in the Al octahedron. The net atomic charges obtained from the two data sets are in good agreement, except for the Al atom. The correlation between κ and P_{val} parameters in the kappa refinements yields a difference in the values of the chemical formula $LiAl(SiO_3)_2$ electrostatic energy estimated from the two data sets.

The financial support of the CNRS and of Université Henri Poincaré, Nancy 1, France, is gratefully acknowledged. We are grateful to Professor Y. Dusausoy for the sample of spodumene and the clarification of structural and mineralogical aspects. We wish to thank Professor C. Lecomte, Dr N. K. Hansen and Dr R. H. Blessing for fruitful discussion of the results.

References

Becker, P. J. & Coppens, P. (1974). *Acta Cryst.* A**30**, 129–147.
Becker, P. J. & Coppens, P. (1990). *Acta Cryst.* A**46**, 254–258.
Bethe, H. A. (1928). *Ann. Phys. (Leipzig)*, **87**, 55–128.
Blessing, R. H. (1987). *Crystallogr. Rev.* **1**, 3–58.
Blessing, R. H. (1989). *J. Appl. Cryst.* **22**, 396–397.
Blessing, R. H. (1995). *Acta Cryst.* A**51**, 33–38.
Cameron, M., Sueno, S., Prewitt, C. T. & Papike, J. J. (1973). *Am. Mineral.* **58**, 594–618.
Clark, J. R., Appleman, D. E. & Papike, J. J. (1969). *Mineral. Soc. Am. Spec. Pap.* **2**, 31–50.
Clementi, E. & Raimondi, D. L. (1963). *J. Chem. Phys.* **38**, 2686–2689.
Clementi, E. & Roetti, C. (1974). *At. Data Nucl. Data Tables*, **14**, 177–178.
Coppens, P., Guru Row, T. N., Leung, P., Stevens, E. D., Becker, P. J. & Yang, Y. W. (1979). *Acta Cryst.* A**35**, 63–72.
Cruickshank, D. W. J. (1949). *Acta Cryst.* **2**, 65–82.
DeTitta, G. T. (1985). *J. Appl. Cryst.* **18**, 75–79.
Enraf–Nonius (1989). *CAD-4 Diffractometer Software*. Version 5.0. Enraf–Nonius, Delft, The Netherlands.
Fischer, R. X., Lirzin, A., Kassner, D. & Rüdinger, B. (1991). *Z. Kristallogr. Suppl.* **3**, 75.
Gajdardziska-Josifovska, M., McCartney, M. R., de Ruijter, W. J., Smith, D. J., Weiss, J. K. & Zuo, J. M. (1993). *Ultramicroscopy*, **50**, 285–299.
Ghermani, N. E., Bouhmaida, N. & Lecomte, C. (1992). *ELECTROS, STATDENS. Computer Programs to Calculate Electrostatic Properties from High Resolution X-ray Diffraction.* Internal report URA CNRS 809. Université Henri Poincaré, Nancy 1, France.
Ghermani, N. E., Lecomte, C. & Bouhmaida, N. (1993). *Z. Naturforsch. Teil A*, **48**, 91–98.
Ghermani, N. E., Lecomte, C. & Dusausoy, Y. (1996). *Phys. Rev. B*, **53**, 5231–5239.
Gibbs, G. V., Hill, F. C. & Boisen, M. B. Jr (1997). *Phys. Chem. Mineral.* **24**, 167–178.
Graafsma, H., Souhassou, M., Puig-Molina, A., Harkema, S., Kvick, Å. & Lecomte, C. (1998). *Acta Cryst.* B**54**, 193–195.
Graham, J. (1975). *Am. Mineral.* **60**, 919–923.
Hansen, N. K. & Coppens, P. (1978). *Acta Cryst.* A**34**, 909–921.
Ivanov, Yu. V., Belokoneva, E. L., Protas, J., Hansen, N. K. & Tsirelson, V. G. (1998). *Acta Cryst.* B**54**, 774–781.
Johnson, C. K. (1976). *ORTEP*II. Report ORNL-5138. Oak Ridge National Laboratory, Oak Ridge, Tennessee, USA.
Kuntzinger, S., Ghermani, N. E., Dusausoy, Y. & Lecomte, C. (1998). *Acta Cryst.* B**54**, 819–833.
Kurki-Suonio, K. (1977). *Isr. J. Chem.* **16**, 115–123.
Lewis, J., Schwarzenbach, D. & Flack, H. D. (1982). *Acta Cryst.* A**38**, 733–739.
McCandlish, L. E., Stout, G. H. & Andrews, L. C. (1975). *Acta Cryst.* A**31**, 245–249.
O'Keeffe, M. (1979). *Acta Cryst.* A**35**, 776–779.
O'Keeffe, M. & Spence, J. C. H. (1994). *Acta Cryst.* A**50**, 33–45.
Parker, S. C., Catlow, C. R. A. & Cormack, A. N. (1984). *Acta Cryst.* B**40**, 200–208.
Preuss, E., Linden, G. & Peuckert, M. (1985). *J. Phys. Chem.* **89**, 2955–2961.
Prince, E. (1994). *Mathematical Techniques in Crystallography and Materials Science*, 2nd ed., pp. 107–111. Berlin, Heidelberg, New York, London, Paris, Tokyo, Hong Kong, Barcelona, Budapest: Springer-Verlag.
Rees, B. (1976). *Acta Cryst.* A**32**, 483–488.
Sasaki, S., Fujino, K., Takéuchi, Y. & Sadanaga, R. (1980). *Acta Cryst.* A**36**, 904–915.
Sheu, H. S., Wu, J. C., Wang, Y. & English, R. B. (1996). *Acta Cryst.* B**52**, 458–464.
Spackman, M. A. & Stewart, R. F. (1981). *Chemical Applications of Atomic and Molecular Electrostatic Potentials*, edited by P. Politzer and D. G. Truhlar, p. 407. New York: Plenum.
Spackman, M. A. & Weber, H. P. (1988). *J. Phys. Chem.* **92**, 794–796.
Stewart, R. F. (1979). *Chem. Phys. Lett.* **67**, 335–342.
Stewart, R. F. (1982). *God. Jugosl. Cent. Kristalogr.* **17**, 1–24.
Streltsov, V. A., Belokoneva, E. L., Tsirelson, V. G. & Hansen, N. K. (1993). *Acta Cryst.* B**49**, 147–153.
Wal, R. J. van der, Vos, A. & Kirfel, A. (1987). *Acta Cryst.* B**43**, 132–143.
Williams, D. E. (1989). *Crystallogr. Rev.* **2**, 163–166.